



# Synaptic Effect of A $\delta$ -Fibers by Pulse-Train Electrical Stimulation

Shota Tanaka<sup>1</sup>, Jose Gomez-Tames<sup>1,2</sup>, Koji Inui<sup>3,4</sup>, Shoogo Ueno<sup>2,5</sup>, Akimasa Hirata<sup>1,2,6</sup> and Toshiaki Wasaka<sup>1,2\*</sup>

<sup>1</sup> Department of Electrical and Mechanical Engineering, Nagoya Institute of Technology, Nagoya, Japan, <sup>2</sup> Center of Biomedical Physics and Information Technology, Nagoya Institute of Technology, Nagoya, Japan, <sup>3</sup> Department of Functioning and Disability, Aichi Developmental Disability Center, Institute for Developmental Research, Kasugai, Japan, <sup>4</sup> Department of Integrative Physiology, National Institute for Physiological Sciences, Okazaki, Japan, <sup>5</sup> Department of Biomedical Engineering, Graduate School of Medicine, The University of Tokyo, Tokyo, Japan, <sup>6</sup> Frontier Research Institute for Information Science, Nagoya Institute of Technology, Nagoya, Japan

## OPEN ACCESS

### Edited by:

Mario I. Romero-Ortega,  
University of Houston, United States

### Reviewed by:

Vassilij Tsytarev,  
University of Maryland, College Park,  
United States

Xin Liu,  
University of California, San Diego,  
United States

### \*Correspondence:

Toshiaki Wasaka  
wasaka.toshiaki@nitech.ac.jp

### Specialty section:

This article was submitted to  
Neural Technology,  
a section of the journal  
Frontiers in Neuroscience

**Received:** 18 December 2020

**Accepted:** 29 March 2021

**Published:** 26 April 2021

### Citation:

Tanaka S, Gomez-Tames J, Inui K,  
Ueno S, Hirata A and Wasaka T  
(2021) Synaptic Effect of A $\delta$ -Fibers by  
Pulse-Train Electrical Stimulation.  
*Front. Neurosci.* 15:643448.  
doi: 10.3389/fnins.2021.643448

Electrical stimulation of specific small fibers (A $\delta$ - and C-fibers) is used in basic studies on nociception and neuropathic pain and to diagnose neuropathies. For selective stimulation of small fibers, the optimal stimulation waveform parameters are an important aspect together with the study of electrode design. However, determining an optimal stimulation condition is challenging, as it requires the characterization of the response of the small fibers to electrical stimulation. The perception thresholds are generally characterized using single-pulse stimulation based on the strength-duration curve. However, this does not account for the temporal effects of the different waveforms used in practical applications. In this study, we designed an experiment to characterize the effects of multiple pulse stimulation and proposed a computational model that considers electrostimulation of fibers and synaptic effects in a multiscale model. The measurements of perception thresholds showed that the pulse dependency of the threshold was an exponential decay with a maximum reduction of 55%. In addition, the frequency dependence of the threshold showed a U-shaped response with a reduction of 25% at 30 Hz. Moreover, the computational model explained the synaptic effects, which were also confirmed by evoked potential recordings. This study further characterized the activation of small fibers and clarified the synaptic effects, demonstrating the importance of waveform selection.

**Keywords:** intraepidermal electrical stimulation, small fibers, A $\delta$ -fiber, perception/pain, electromagnetic model, nerve model, synaptic model, multiscale model

## INTRODUCTION

The central nervous system receives somatosensory information from different receptors and peripheral nerve fibers, which are integrated by synaptic processes. Free nerve endings or terminals of small fibers, such as the A $\delta$ - and C-fibers, are located in the epidermis. Selective stimulation is essential for investigating somatosensory submodality and pain processes (Vallbo et al., 1979). Intraepidermal electrical stimulation (IES) using a small concentric bipolar needle electrode that injects a current of a few mA to generate a focal electric field around the electrodes can selectively stimulate small fibers (Inui and Kakigi, 2012). Different stimulation parameters (for example,

duration, interstimulus interval, waveform, and electrode polarity) have been proposed to facilitate the selective stimulation of A $\delta$ - and C-fibers. Stimulation of different types of small fibers can be confirmed by measuring the reaction times and recording pain-related evoked potentials (Inui and Kakigi, 2012; Kodaira et al., 2014; Hugosdottir et al., 2019). However, defining the optimal stimulation conditions for these small fibers is challenging as they depend on the design of the electrode, characteristics of the stimulated fibers, and how the information is integrated into the synaptic process on the spinal cord and cognitive levels (Inui et al., 2005; Otsuru et al., 2009).

The first approach to characterize the stimulation of small fibers is the strength-duration relationship approach (S-D curve), which shows the threshold relationship between pulse amplitude and duration. The electrostimulation threshold becomes small with an increase in pulse duration until its convergence to a minimum value termed “rheobase.” Two studies measured the perception threshold to derive S-D curves but were not specific to a particular small fiber type (co-activation of different small fibers) (Hennings et al., 2017; Poulsen et al., 2020). Electromagnetic dosimetry has also been used to evaluate the internal electric field as a metric of stimulation in the skin region where the fibers are located (Mørch et al., 2011; Frahm et al., 2013; Hirata et al., 2013a; Motogi et al., 2016).

The effects of the computed internal electric field on the small fiber models were considered. Poulsen et al. (2020) used a fiber model to estimate the activation threshold with matching S-D curve measurements for a limited number of pulse durations. For simplicity, the computed thresholds of a single fiber model were assumed to be equal to the perception threshold based on *in vivo* experiments. In our previous study (Tanaka et al., 2021), the A $\delta$ -fiber model was characterized based on S-D measurements considering the region where multiple fibers could be stimulated. These multiscale models (skin volume conductor and neural models) described local responses at fiber terminals and helped us to better understand the mechanism of IES for single-pulse stimulation. However, they were not sufficient to describe the perception thresholds for non-single-pulse stimulation, wherein the synaptic process became relevant.

Synaptic models incorporate afferent information in the form of temporal/spatial summation to describe variations in the postsynaptic membrane potential (Roth and van Rossum, 2013; Heshmat et al., 2020). If the membrane potential reaches a threshold, the postsynaptic neuron is fired. Experiments on the primary motor have shown that the motor threshold changes with the stimulation waveform (Lilly et al., 1952; Taniguchi et al., 1993), and its effects have been replicated by adopting multiscale modeling with a conductance-based synaptic model (Gomez-Tames et al., 2018, 2019). These complex factors need to be further characterized for peripheral stimulation to optimize protocols for selective stimulation of small fibers.

The present study aimed to measure and characterize the effects of stimulation of a train of pulses on the perception threshold via stimulation of A $\delta$ -fibers *in vivo* for the first time. Stimulation of A $\delta$ -fibers and synaptic effects were confirmed by the reaction time and evoked potential measurements. In addition, we present a synaptic model that integrates the

responses of the A $\delta$ -fiber information via a comparison with experiments. One of the features of this study is that the computational model combines electromagnetic dosimetry and nerve activation modeling to integrate the propagation pulses descending from the fiber terminal into a synaptic model.

## MODEL AND METHODS

### The IES Experiment

We measured the perception threshold for pulse-train electrical current stimulation with a variable number of pulses (with a fixed frequency) and frequencies (with a fixed number of pulses). The number of healthy participants was eight (age  $20.8 \pm 1.2$  years, five females) and nine (age  $21.6 \pm 1.3$  years, two females) for pulse number and frequency variation, respectively. The experiments were approved by the Ethical Committee of the Nagoya Institute of Technology (no. 29–014).

The stimulation device (STG4004, Multi-Channel Systems GmbH, Germany) delivered multiple square pulse currents through a concentric bipolar needle electrode (NM-983 W, Nihon Kohden, Tokyo, Japan). The inner needle and ring electrodes were assigned as the anode and cathode of the stimulation device, respectively. The stimulation was applied to the dorsum of the left hand to stimulate A $\delta$ -fibers, as shown in **Figure 1**. The number of pulses varied from 1 to 10 (one pulse step) using a frequency of 30 Hz. We then evaluated the frequency from 10 Hz to 200 Hz (nine frequencies) using six pulses. The conditions were selected randomly for the experiments.

The experimental protocol to measure the perception threshold (the lowest current to generate sensation in participants) was presented in our previous study (Tanaka et al., 2021). In brief, the participants were instructed to press a button as soon as they felt the sensation. The time between stimulus onset and detection, by pressing a button (termed reaction time), was automatically recorded. The method of limits was used to determine the threshold of the stimulus with consecutive ascending and descending trials. The threshold was considered to be detected when the participant reported a sensation at least two of three times with reaction time in the range of A $\delta$ -fiber transmission (200 to 800 ms) (Rag e et al., 2010; Kodaira et al., 2014).

### Pain-Related Evoked Potentials by A $\delta$ -Fiber

In order to confirm the activation of A $\delta$ -fibers and synaptic effect, we measured the pain-related evoked potentials of A $\delta$ -fibers by electroencephalography (EEG) recordings in three healthy participants (age,  $23.3 \pm$  years, all-males) and two healthy participants (age,  $22.5 \pm 1.5$  years, all-males), respectively. First, we confirmed the pain-related evoked potentials of A $\delta$ -fibers for single-pulse stimulation using different pulse widths (60, 100, 200, 400, 800, and 1600  $\mu$ s). Second, we demonstrated the synaptic effect by recording pain-related evoked potentials for pulse-train electrical stimulation with a different number of pulses using a fixed stimulus injection current. The selected injection current amplitude corresponded to the perception

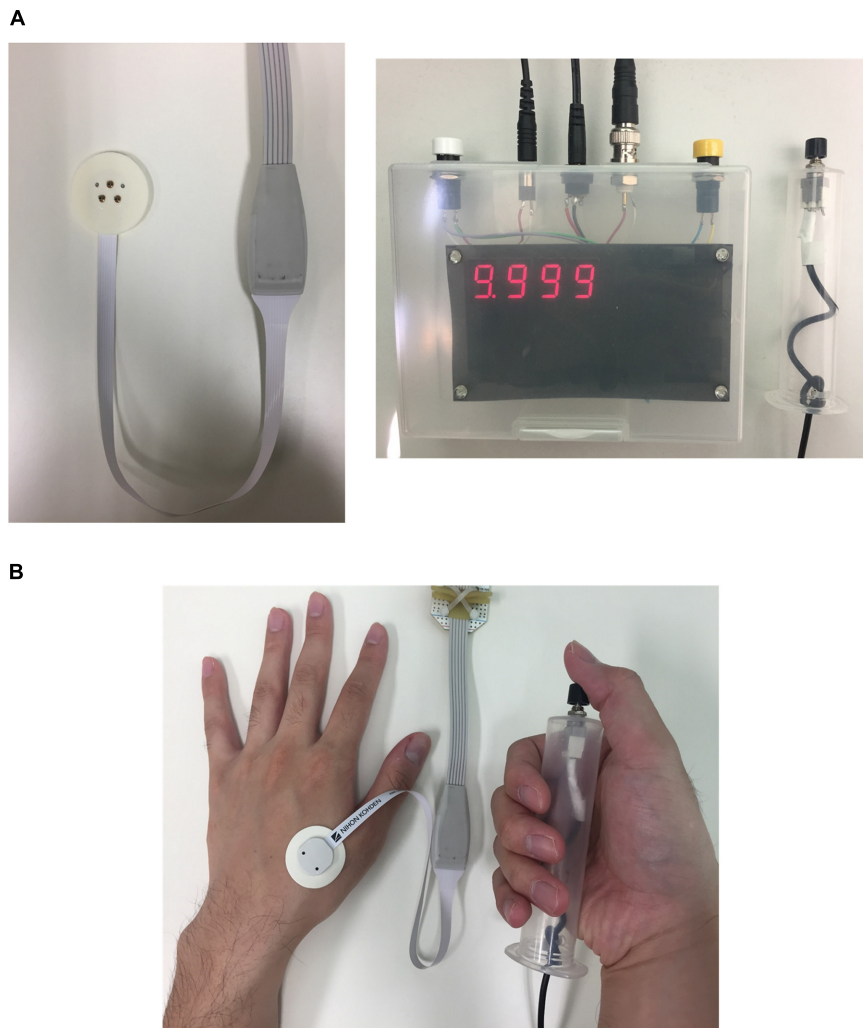


**FIGURE 1** | Experimental setup: **(A)** concentric bipolar electrode needle and measurement equipment of reaction time (time between stimulation and detection of sensation) and **(B)** photo of a participant pressing the push-button during perception threshold detection experiment.

threshold for eight consecutive pulses. We then investigated the presence or absence of pain-related evoked potentials when fewer pulses were applied (two, four, and six).

The protocol for EEG recording following each stimulus condition was described. The active electrode was placed at the Cz of the International 10–20 system and referred to as the linked earlobes (A1–A2). We focused on the cortical response recorded from the Cz since a previous study showed that the maximum response following noxious stimuli was recorded from the Cz (Kakigi et al., 1989). The impedance of the electrode was less than 5 k $\Omega$ . In addition, a pair of electrodes placed supra- and infra-orbitally to the left eye was used to record the electrooculogram (EOG). The EEG signals were recorded with a band-pass filter (0.5 to 30 Hz) at a sampling rate of 1000 Hz. The EEG signals were then averaged from the 20 stimuli applied in each pulse condition. Epochs in which the signal variations were larger than 80  $\mu$ V in the EEG and EOG were excluded. Thereafter, a total of 10–15 stimuli were averaged for each condition. The

analysis was conducted from 100 ms before to 800 ms after the onset of the IES. We used the 100 ms period before stimulation as the baseline. For the peak determination of the waveform, we adopted a threshold of more than three times the standard deviation calculated from the prestimulus period. During the EEG recording, we instructed the participant not to pay attention to noxious stimuli in order to eliminate the attentional effect. After the EEG recordings, we asked the participants if they felt any noxious sensation. The participants reported that they felt slight pain with 6- and 8-pulse stimulation, but no pain with fewer pulses.

### Multiscale Modeling of A $\delta$ -Fibers

A computational multiscale electromagnetic model of A $\delta$ -fibers during IES was developed in our previous studies (Motogi et al., 2016; Tanaka et al., 2021). This was based on strength-duration measurements using single-pulse stimulation. A summary of the results is provided in this section. In section “Synaptic Model,” a

model of the synapse is incorporated to describe the pulse-train stimulation of small fibers for the first time.

### Skin Volume Conductor Modeling

The electrical skin model is treated as a passive volume conductor to compute the *in situ* electric field produced by the injection current. The skin was modeled as a layered structure for hairy skin (Alekseev and Ziskin, 2007; Schmid et al., 2013; De Santis et al., 2015; Motogi et al., 2016). The thickness of the tissues and their conductivity values were identical to those observed in our previous studies and are summarized in **Figure 2A** (Tanaka et al., 2021). The dimensions of the skin model were 1.54 mm (depth)  $\times$  1.65 mm  $\times$  1.65 mm discretized by voxels of 5  $\mu$  m in length.

The scalar potential finite difference method (Dawson and Stuchly, 1996) was used to numerically solve the following equation to obtain the scalar potential  $\phi$  considering that the frequency is below the kHz range and displacement current is negligible (Hirata et al., 2013b):

$$\nabla(\sigma \nabla(\phi)) = 0 \quad (1)$$

where  $\sigma$  is the conductivity of the tissue. The potential was solved iteratively using the successive-over-relaxation and multigrid methods (Laakso and Hirata, 2012). A current source was connected between the inner and outer rings of the bipolar needle electrode (Motogi et al., 2014). The inner electrode and ring electrode corresponded to the cathode and anode, respectively, and were modeled as perfect conductors. To obtain the *in situ* electric fields, the potential difference between the nodes of the voxel was divided by the voxel length.

### Nerve Activation Modeling for A $\delta$ -Fibers

The effects of the extracellular electric field derived from Eq. (1) on myelinated nerve fibers were described using the following general equation (McNeal, 1976; Rattay, 1999):

$$\begin{aligned} C_{m,n} \frac{dV_{m,n}}{dt} + I_{ion,n} - \frac{V_{m,n-1} - 2V_{m,n} - 2V_{m,n+1}}{0.5(R_{m,i} + R_{m,n})} \\ = \frac{V_{e,n-1} - 2V_{e,n} - 2V_{e,n+1}}{0.5(R_{m,i} + R_{m,n})} \end{aligned} \quad (2)$$

where  $C_m$  is the membrane capacitance, and  $R_{m,i}$  and  $R_{m,n}$  are the internode membrane resistivity and nodal membrane resistivity, respectively. The membrane potential is represented by  $V_m$ , where  $n = V_e - V_i$ . The fibers are formed by internodes (myelin segments) and nodes of Ranvier (ionic channels). At the internodes, the membrane current  $I_{ion,n}$  was modeled by the passive conductance multiplied by the membrane potential. At the nodes of Ranvier, the ionic membrane current was formulated using a modified Chiu-Ritchie-Rogart-Stagg-Sweeney model, which is a conductance-based voltage-gated model (Sweeney et al., 1987).

The parameters in the modified fiber model were explored in the electromagnetic computation model based on reported values in the literature (depth and diameter) (MacIver and Tanelian, 1993; Reilly et al., 1997) to fit the experimental strength-duration experiment for single-pulse stimulation. The area of

stimulation was estimated based on the rheobase value of the strength-duration experiment. The conductance and capacitance of the cable equation were modified to adjust the chronaxie value (Sweeney et al., 1987) using the least-square error for each pulse.

### Synaptic Model

We integrated the responses of the A $\delta$ -fiber model into a synaptic model to investigate the synaptic effects of pulse-train electrical stimulation, as shown in **Figure 2B**. The generated spikes (namely, action potentials) from A $\delta$ -fibers in the skin produced an excitatory postsynaptic current (EPSC) in the postsynaptic membrane. The EPSC produces a variation in the transmembrane potential of the postsynaptic neuron that can generate an action potential if the membrane potential reaches a minimum threshold. To obtain the EPSC, we first modeled the synaptic conductance as the sum of two exponentials (Roth and van Rossum, 2013):

$$g_j = g_{max,j} f \left( e^{-\frac{t}{\tau_{r,j}}} - e^{-\frac{t}{\tau_{f,j}}} \right) \quad (3)$$

where  $g_{max,j}$  is the peak conductance, and  $\tau_{r,j}$  and  $\tau_{f,j}$  are the rise and fall time constants, respectively. The normalization factor  $f$  (Roth and van Rossum, 2013) is set such that the amplitude is equal to  $g_{max,j}$ .

The total synaptic conductance  $g_{total}$  is calculated by combining the effects of each synapse  $j$  as the convolution of the synaptic conductance  $g_j$  at time  $t_x$  and the spike sequences  $s_j$  arriving from the presynaptic neuron (A $\delta$ -fibers), as follows:

$$g_{total}(t_x) = \sum_{j=0}^J w_j \int_0^{t_x} s_j(\tau) g_j(t_x - \tau) d\tau \quad (4)$$

where  $J$  is the total number of presynaptic neurons (A $\delta$ -fibers), and  $s_j$  is the delta pulse. The parameter  $w_j$  is a weighting term, meaning the probability of depolarizing the synapse before the input and generating action potentials.

Then, the EPSC is given as follows:

$$EPSC(t_x) = g_{total}(t_x) [E - V_m(t_x)] \quad (5)$$

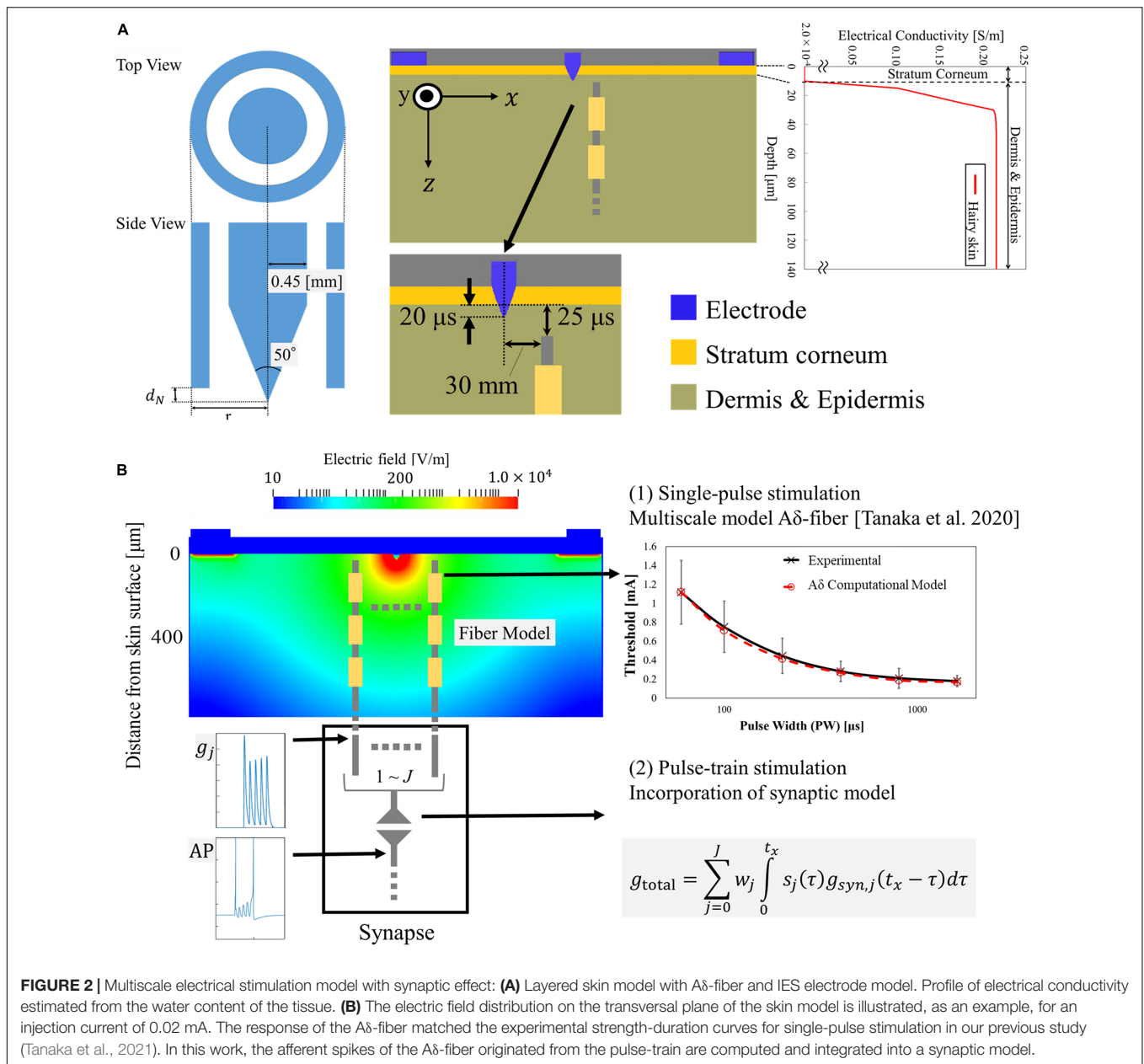
where  $E$  is the synaptic reversal potential, and  $V_m$  is the postsynaptic membrane potential. We evaluated the synaptic responses in a postsynaptic neuron using an Izhikevich spike model (Izhikevich, 2003), as follows:

$$\frac{dV_m}{dt} = 0.04V_m^2 + 5V_m + 140 - u + EPSC \quad (6)$$

$$\frac{du}{dt} = 0.02(0.2V_m - u) \quad (7)$$

Where  $u$  is the membrane recovery variable.

In this study, we investigated the number of presynaptic inputs (number of individual fibers) required to activate postsynaptic neurons under different train-pulse conditions. We then used the relationship between the current threshold and the number of presynaptic neurons to obtain the injection current threshold to



activate the postsynaptic neuron (Supplementary Figure 1), as described in section “Development of a Computational Synaptic Model.” This approach has been used in synaptic models for brain stimulation of the motor area (Gomez-Tames et al., 2019).

## EXPERIMENTAL AND COMPUTATIONAL RESULTS

### Experiment Results of Aδ-Fibers for Pulse-Train Electrical Stimulation

The injection current threshold to generate pain perception via Aδ-fibers was experimentally obtained for pulse-train electrical

stimulation at a fixed frequency (30 Hz). As shown in Figure 3A, the threshold decreased with an increase in the pulse number and converged after five consecutive pulses. The synaptic effect generated a reduction of the threshold by 2.3 times for multiple-pulse stimulation of five or more consecutive pulses to a single pulse. Higher variability was observed for a few pulses due to intrinsic skin morphology and needle depth variability in the experiments, which will be discussed below. Thus, the measured perception thresholds were normalized by the average of the thresholds from six to ten pulses (Figure 3B). The reaction time of the volunteers in Table 1 requires more time for a larger number of pulses.

The dependence of the threshold was also investigated for frequency (10 Hz to 200 Hz), as shown in Figure 4A

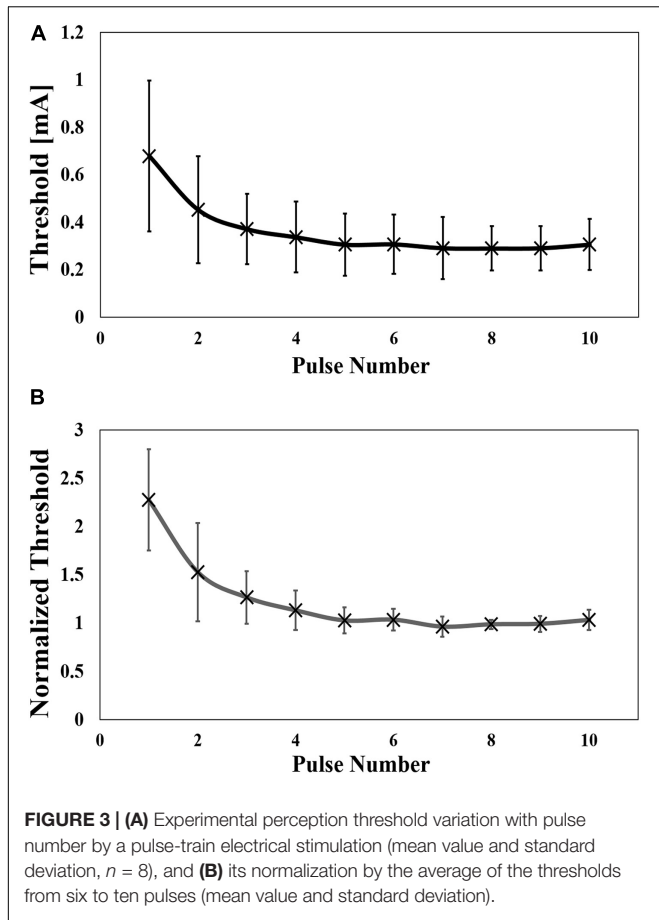


**FIGURE 3 | (A)** Experimental perception threshold variation with pulse number by a pulse-train electrical stimulation (mean value and standard deviation,  $n = 8$ ), and **(B)** its normalization by the average of the thresholds from six to ten pulses (mean value and standard deviation).

**TABLE 1 |** The reaction time of perception threshold at a different number of pulses and frequencies.

Pulse number	Reaction time [s] (Mean ± SD)	Frequency [Hz]	Reaction time [s] (Mean ± SD)
1	0.521 ± 0.112	10	0.642 ± 0.060
2	0.487 ± 0.073	20	0.586 ± 0.087
3	0.496 ± 0.088	30	0.508 ± 0.078
4	0.559 ± 0.126	40	0.508 ± 0.041
5	0.606 ± 0.124	50	0.479 ± 0.054
6	0.615 ± 0.110	60	0.490 ± 0.117
7	0.641 ± 0.059	80	0.484 ± 0.098
8	0.631 ± 0.069	100	0.427 ± 0.083
9	0.609 ± 0.063	200	0.422 ± 0.094
10	0.641 ± 0.113		

SD, standard deviation.

for six pulses. The mean value of the minimum threshold was found at 30 Hz (10 Hz and 80 Hz), which converged at a mean frequency of 120 Hz (80 Hz to 200 Hz). The threshold was reduced by up to 26% of the maximum value. To reduce the intrinsic variability in the experiments, the threshold was normalized by the mean value of the converged threshold, which was defined as the threshold at a frequency

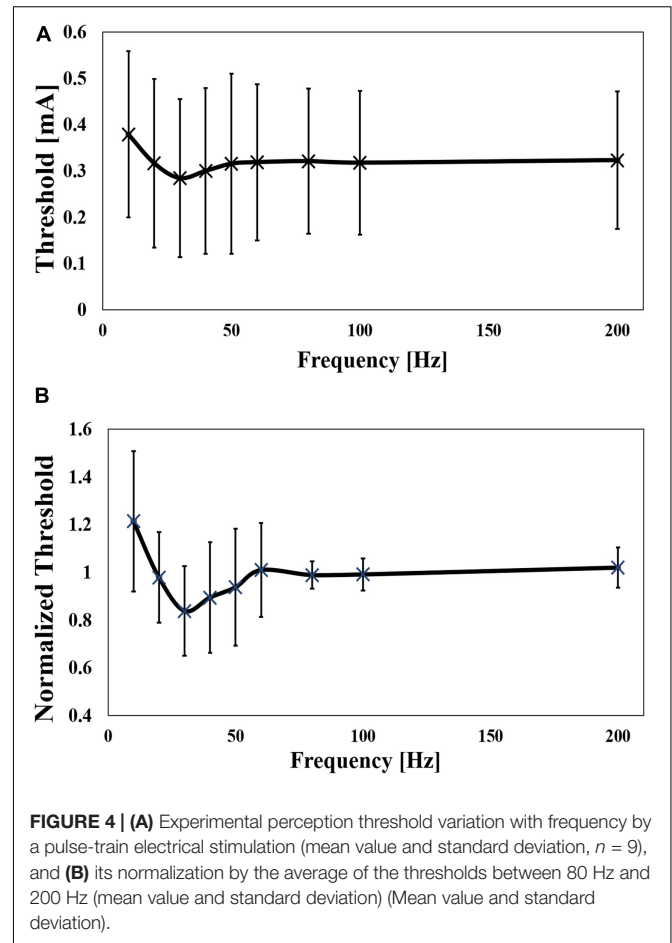


**FIGURE 4 | (A)** Experimental perception threshold variation with frequency by a pulse-train electrical stimulation (mean value and standard deviation,  $n = 9$ ), and **(B)** its normalization by the average of the thresholds between 80 Hz and 200 Hz (mean value and standard deviation) (Mean value and standard deviation).

**TABLE 2 |** Experimental threshold and peak latency of pain-related evoked potentials by single-pulse stimulation (mean value and standard deviation,  $n = 3$ ).

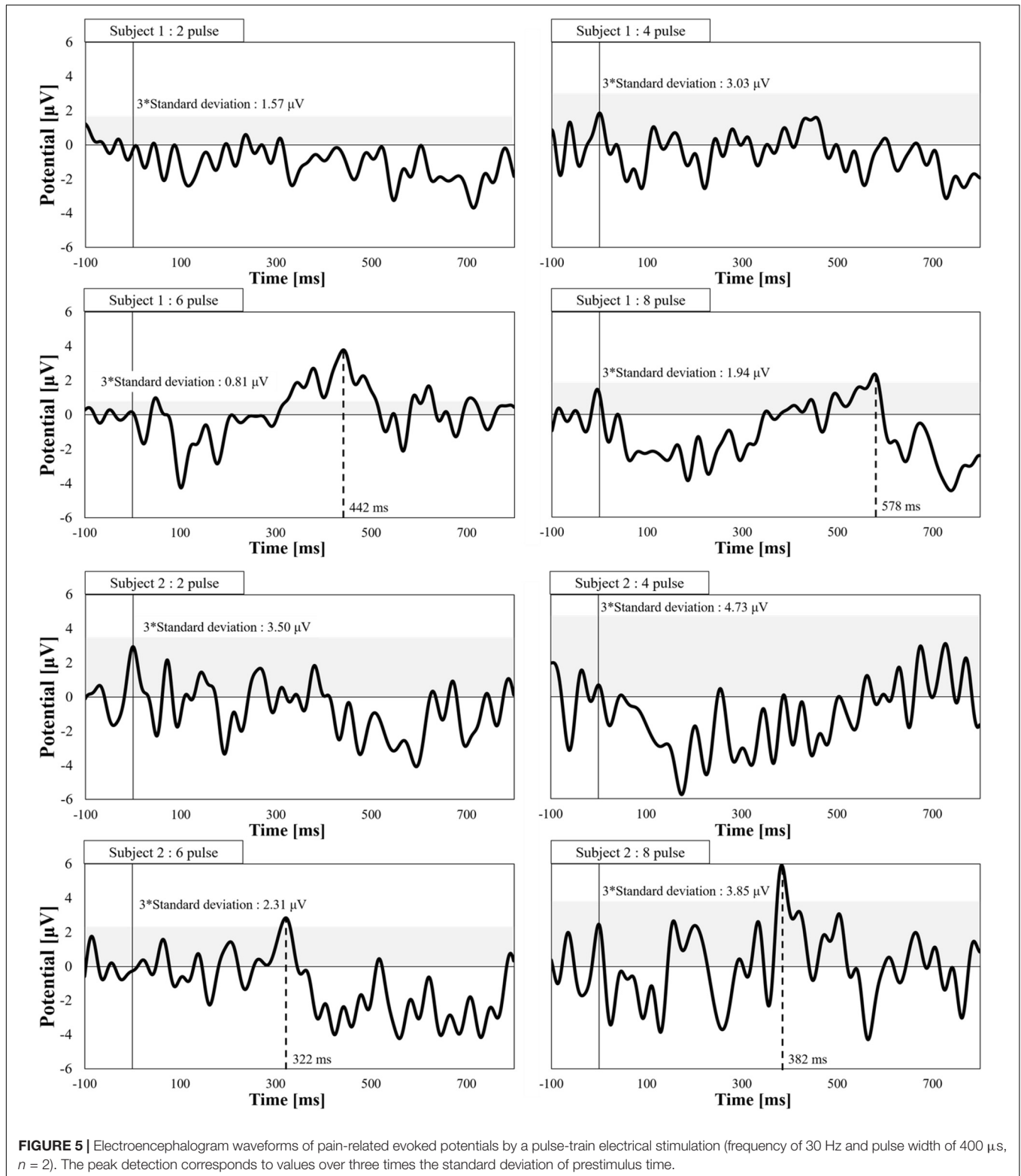
Pulse width (μs)	Threshold [mA] (Mean ± SD)	Reaction time by evoked potential latency [s] (Mean ± SD)
60	0.983 ± 0.152	0.363 ± 0.020
100	0.647 ± 0.084	0.364 ± 0.085
200	0.487 ± 0.021	0.330 ± 0.039
400	0.330 ± 0.045	0.370 ± 0.035
800	0.323 ± 0.021	0.380 ± 0.101
1600	0.257 ± 0.049	0.391 ± 0.015

SD, standard deviation.

of 80 Hz to 200 Hz (**Figure 4B**). The normalized curve shows a clear tendency, confirming the bottom peak at 30 Hz. As shown in **Table 1**, the reaction time was slower at lower frequencies.

### Verification of Aδ-Fibers and Synaptic Effect by Evoked Potentials

We detected evoked potentials from Aδ-fiber stimulation using single-pulse stimulation. **Table 2** shows the peak latency of pain-related evoked potentials that were not significantly affected



by pulse width (330–390 ms). These reaction times were faster than those when the participant pressed the button under the same conditions in our previous study (470 ms to 520 ms) (Tanaka et al., 2021).

We also verified synaptic effects using evoked potential measurements. **Figure 5** shows the evoked potentials for different numbers of consecutive stimulation pulses. The stimulation amplitude was fixed for all conditions (perception threshold of

eight pulses). We observed pain-related evoked potentials at eight and six pulses, but not for two or four pulses, which agrees with the higher stimulation intensities for fewer pulses, as observed in **Figure 3**.

## Development of a Computational Synaptic Model

The electrical parameters of the synaptic model were found to coincide with the experimental data shown in **Figure 3**. The least-squares error between the experimental and computational results was adopted.

The synaptic model considers the effect of the number of activated presynaptic neurons (estimated computationally by the multiscale model of A $\delta$ -fibers in section “Multiscale Modeling of A $\delta$ -Fibers”) and their afferent spike sequence (number of stimulating pulses). Both inputs were used to determine the activation of postsynaptic neurons using a synaptic model. The parameters of the synaptic model are as follows: synaptic weight ( $w$ ), rise time ( $\tau_r$ ), and fall time ( $\tau_f$ ).

First, more fibers are activated at higher injection current as the region where activation occurred became larger (broader and deeper) from a biophysical perspective. The number of stimulated fibers was estimated using the multiscale A $\delta$ -fiber model for different injection currents, considering a uniform fiber density (Ebenezer et al., 2007). Thereafter, the relationship between the number of fibers and injection current was obtained, as shown in Appendix A. Next, the synaptic weight was determined so that the estimated number of fibers activate the postsynaptic neuron under single-pulse stimulation condition (no synaptic effect condition). Second, the number of fibers (corresponding to the current amplitude of the IES) required to activate the postsynaptic neuron was computed for different numbers of train pulses. The required number of fibers to activate the postsynaptic neuron was used to determine the perception thresholds based on the relationship between the number of fibers and the injection current. Third, the parameters  $\tau_r$  and  $\tau_f$  were adjusted to fit the experimental thresholds for each number of pulses, as shown in **Figure 3**. The fitted parameters of the synaptic model are presented in **Table 3**.

The computational results for the perception threshold are shown in **Figure 6**. The computed perception threshold corresponded to the injection current (IES) required to activate the postsynaptic neuron (that is, eliciting an action potential) using the integrated multiscale model of A $\delta$ -fibers with the synaptic model with different numbers of stimulation pulses. A good match to the experimental results was obtained by changing the relatively small space parameter of the synaptic model. The mean error was 14  $\mu$  A.

## DISCUSSION

In this study, perception thresholds via selective stimulation of A $\delta$ -fibers were measured using pulse-train stimulation. We hypothesized that a train of pulses can modify the perception threshold via synaptic effects. We observed threshold dependency

**TABLE 3** | Estimated synaptic model parameters based on the measured results.

Parameter	Value
Number of fibers at a single pulse	71
Rise time constant ( $\tau_r$ )	4.0 ms
Fall time constant ( $\tau_f$ )	5.0 ms
Synapse weight ( $w$ )	$8.1 \times 10^{-3}$

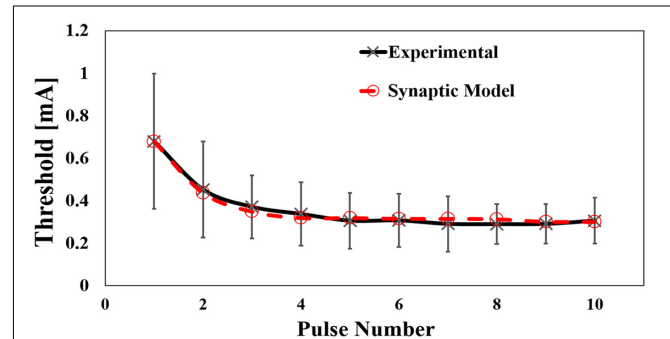


**FIGURE 6** | Computed results of the effect of pulse number by pulse-train electrical stimulation (experimental mean value and standard deviation,  $n = 8$ ).

on the number of pulses and the frequency variation. We then proposed a computational model for synaptic effects.

In the first experiment, we observed that an increase in the number of pulses decreased the threshold by approximately 2.7 times. This is attributed to a synaptic effect on the postsynaptic neurons in the ventral horn of the spinal cord as the number of afferent pulses is increased, and temporal summation explains the reduction in the measured threshold. We found that after a certain number of pulses (six pulses in our experiment), the threshold converged to a minimum. We considered that the postsynaptic neuron reaches the membrane potential threshold at this number of pulses, and additional pulses will not change the stimulation threshold. Moreover, we discarded any enhancement of the membrane potential of the A $\delta$ -fibers at the terminal close to the needle electrode, considering the fixed frequency of the train-pulse stimulation (Reilly, 1989). In the second experiment, the frequency dependency of the perception threshold was investigated. We observed a U-shaped response with a minimum threshold of approximately 30 Hz and a reduction of 30% from the maximum value. The same phenomenon has been observed for phosphine perception thresholds during transcranial alternating current stimulation (Rohracher, 1935; Turi et al., 2013; Evans et al., 2019). Although the frequency at the minimum value was found to be between 16 Hz and 20 Hz, the difference may be due to the different characteristics of rod visual neurons. Based on the stimulation rate variation, we conjectured that facilitation (temporal/spatial summation) and the fatigue process of the synapse were the reasons for the U-shaped response (frequency variation experiment). The former reduced the stimulation threshold up to a certain stimulation frequency where a fatigue process (for example, depletion of vesicles that contain the neurotransmitter available at the synapses) initiated at higher

rates (Simons-Weidenmaier et al., 2006; Ikeda and Bekkers, 2009). In both experiments we adopted normalization of the thresholds, showing a clear trend due to inter-variability factors (such as needle depth, tissue thickness, and A $\delta$ -fiber distribution).

As an additional demonstration of the response of A $\delta$ -fibers and synaptic effects, EEG recordings were conducted. We observed evoked responses at single pulse with detection time within a range of 0.33 s to 0.39 s (3 m/s) that agrees within conduction velocity of A $\delta$ -fiber and is faster than that of C-fiber (0.5 m/s to 2 m/s) (Weiss et al., 2008), thus confirming the selectivity of A $\delta$ -fiber. In addition, the synaptic effect was confirmed by recording the evoked potential dependency on the number of pulses. As an increasing number of pulses (up to five pulses) reduces the perception threshold, we hypothesized that the evoked potential disappears if the number of pulses is reduced while maintaining the injection current that generates a perception with six pulses. We found that two and four consecutive pulses did not produce an evoked response.

In our recent study, a multiscale model of A $\delta$ -fibers was proposed and verified using S-D measurements for a single pulse condition to estimate perception thresholds (Tanaka et al., 2021). Based on this model, we incorporated a synaptic model to estimate the temporal effects of a train of pulses for the first time. Our multiscale model coupled with a synaptic model explained that a higher number of pulses of the stimulation waveform increased the number of descending pulses on each activated A $\delta$ -fiber, thus facilitating the activation of postsynaptic neurons with fewer presynaptic fibers. Therefore, to activate fewer A $\delta$ -fibers, a smaller injection current was required. A limitation of the proposed model is reproducing the results of the measured threshold under different frequencies. This requires extending the synaptic model to include potential fatigue processes at higher stimulation rates, which needs to be investigated in future work. Finally, the current methodology can be applied to other small fibers, such as C-fibers, in future studies.

## REFERENCES

- Alekseev, S. I., and Ziskin, M. C. (2007). Human Skin Permittivity Determined by Millimeter Wave Reflection Measurements. *Bioelectromagnetics* 28, 331–339. doi: 10.1002/bem.20308
- Dawson, T. W., and Stuchly, M. A. (1996). Analytic Validation of a Three-Dimensional Scalar-Potential Finite-Difference Code for Low-Frequency Magnetic Induction. *Applied Computational Electromagnetics Society Journal* 11, 72–81. \*
- De Santis, V., Chen, X. L., Laakso, I., and Hirata, A. (2015). An Equivalent Skin Conductivity Model for Low-Frequency Magnetic Field Dosimetry. *Biomedical Physics and Engineering Express* 1, 015201. doi: 10.1088/2057-1976/1/1/015201
- Ebenezer, G. J., Hauer, P., Gibbons, C., McArthur, J. C., and Polydefkis, M. (2007). Assessment of Epidermal Nerve Fibers: A New Diagnostic and Predictive Tool for Peripheral Neuropathies. *Journal of Neuropathology and Experimental Neurology*. *Oxford Academic* 66, 1059–1073. doi: 10.1097/nen.0b013e31815c8989
- Evans, I. D., Palmisano, S., Loughran, S. P., Legros, A., and Croft, R. J. (2019). Frequency-Dependent and Montage-Based Differences in Phosphene Perception Thresholds via Transcranial Alternating Current Stimulation. *Bioelectromagnetics* 40, 365–374.
- Frahm, K. S., Mørch, C. D., Grill, W. M., Lubock, N. B., Hennings, K., and Andersen, O. K. (2013). Activation of Peripheral Nerve Fibers by Electrical

## DATA AVAILABILITY STATEMENT

The raw data supporting the conclusions of this article will be made available by the authors, without undue reservation.

## ETHICS STATEMENT

The studies involving human participants were reviewed and approved by Ethical Committee of the Nagoya Institute of Technology. The patients/participants provided their written informed consent to participate in this study.

## AUTHOR CONTRIBUTIONS

TW and AH conceived and designed the study. TW and ST conducted the experiments. JG-T and ST conducted the simulation experiments. TW, ST, and JG-T processed the data. All authors analyzed the data, wrote the manuscript, and read and approved the manuscript.

## FUNDING

This work was supported by the Ministry of Internal Affairs and Communications (Grant Number JPMI10001).

## SUPPLEMENTARY MATERIAL

The Supplementary Material for this article can be found online at: <https://www.frontiersin.org/articles/10.3389/fnins.2021.643448/full#supplementary-material>

- Stimulation in the Sole of the Foot. *BMC Neuroscience* 14:116. doi: 10.1186/1471-2202-14-116
- Gomez-Tames, J., Hirata, A., Tamura, M., and Muragaki, Y. (2019). Corticomotoneuronal Model for Intraoperative Neurophysiological Monitoring During Direct Brain Stimulation. *International Journal of Neural Systems* 29, 1850026. doi: 10.1142/S0129065718500260
- Gomez-Tames, J., Kutsuna, T., Tamura, M., Muragaki, Y., and Hirata, A. (2018). Intraoperative Direct Subcortical Stimulation: Comparison of Monopolar and Bipolar Stimulation. *Physics in Medicine & Biology* 63, 225013. doi: 10.1088/1361-6560/aaea06
- Hennings, K., Frahm, K. S., Petrini, L., Andersen, O. K., Arendt-Nielsen, L., and Mørch, C. D. (2017). Membrane Properties in Small Cutaneous Nerve Fibers in Humans. *Muscle & Nerve* 55, 195–201. doi: 10.1002/mus.25234
- Heshmat, A., Sajedi, S., Chacko, L. J., Fischer, N., Schrott-Fischer, A., and Rattay, F. (2020). Dendritic Degeneration of Human Auditory Nerve Fibers and Its Impact on the Spiking Pattern Under Regular Conditions and During Cochlear Implant Stimulation. *Frontiers in Neuroscience* 14:599868. doi: 10.3389/fnins.2020.599868
- Hirata, A., Hattori, J., Laakso, I., Takagi, A., and Shimada, T. (2013a). Computation of Induced Electric Field for the Sacral Nerve Activation. *Physics in Medicine and Biology* 58, 7745–7755. doi: 10.1088/0031-9155/58/21/7745
- Hirata, A., Ito, F., and Laakso, I. (2013b). Confirmation of Quasi-Static Approximation in SAR Evaluation for a Wireless Power Transfer System.\*

- Physics in Medicine and Biology* 58, N241–N249. doi: 10.1088/0031-9155/58/17/N241
- Hugosdottir, R., Mørch, C. D., Andersen, O. K., and Arendt-Nielsen, L. (2019). “Electrical Stimulation of Small Cutaneous Nerve Fibers for Investigating Human Pain Mechanisms,” in *Proceedings of the Nordic Baltic Conference on Biomedical Engineering and Medical Physics(NBC)*, (Reykjavik).
- Ikeda, K., and Bekkers, J. M. (2009). Counting the Number of Releasable Synaptic Vesicles in a Presynaptic Terminal. *Proceedings of the National Academy of Sciences of the United States of America* 106, 2945–2950. doi: 10.1073/pnas.0811017106
- Inui, K., and Kakigi, R. (2012). Pain Perception in Humans: Use of Intraepidermal Electrical Stimulation. *Journal of Neurology, Neurosurgery and Psychiatry* 83, 551–556. doi: 10.1136/jnnp-2011-301484
- Inui, K., Tsuji, T., and Kakigi, R. (2005). Temporal Analysis of Cortical Mechanisms for Pain Relief by Tactile Stimuli in Humans. *Cerebral Cortex* 16, 355–365. doi: 10.1093/cercor/bhi114
- Izhikevich, E. M. (2003). Simple Model of Spiking Neurons. *IEEE Transactions on Neural Networks* 14, 1569–1572. doi: 10.1109/TNN.2003.820440
- Kakigi, R., Shibasaki, H., and Ikeda, A. (1989). Pain-Related Somatosensory Evoked Potentials Following CO<sub>2</sub> Laser Stimulation in Man. *Electroencephalography and Clinical Neurophysiology/Evoked Potentials Section* 74, 139–146.
- Kodaira, M., Inui, K., and Kakigi, R. (2014). Evaluation of Nociceptive A $\delta$ - and C-Fiber Dysfunction with Lidocaine Using Intraepidermal Electrical Stimulation. *Clinical Neurophysiology* 125, 1870–1877. doi: 10.1016/j.clinph.2014.01.009
- Laakso, I., and Hirata, A. (2012). Fast Multigrad-Based Computation of the Induced Electric Field for Transcranial Magnetic Stimulation. *Physics in Medicine and Biology* 57, 7753–7765. doi: 10.1088/0031-9155/57/23/7753
- Lilly, J. C., Austin, G. M., and Chambers, W. W. (1952). Threshold Movements Produced by Excitation of Cerebral Cortex and Efferent Fibers with Some Parametric Regions of Rectangular Current Pulses (Cats and Monkeys). *Journal of Neurophysiology* 15, 319–341.
- MacIver, M. B., and Tanelian, D. L. (1993). Structural and Functional Specialization of A $\delta$  and C Fiber Free Nerve Endings Innervating Rabbit Corneal Epithelium. *Journal of Neuroscience* 13, 4511–4524. doi: 10.1523/jneurosci.13-10-04511.1993
- McNeal, D. R. R. (1976). Analysis of a Model for Excitation of Myelinated Nerve. *IEEE Transactions on Biomedical Engineering* 4, 329–337.
- Mørch, C. D., Hennings, K., and Andersen, O. K. (2011). Estimating Nerve Excitation Thresholds to Cutaneous Electrical Stimulation by Finite Element Modeling Combined with a Stochastic Branching Nerve Fiber Model. *Medical and Biological Engineering and Computing* 49, 385–395. doi: 10.1007/s11517-010-0725-8
- Motogi, J., Kodaira, M., Muragaki, Y., Inui, K., and Kakigi, R. (2014). Cortical Responses to C-Fiber Stimulation by Intra-Epidermal Electrical Stimulation: An MEG Study. *Neuroscience Letters* 570, 69–74.
- Motogi, J., Sugiyama, Y., Laakso, I., Hirata, A., Inui, K., Tamura, M., et al. (2016). Why Intra-Epidermal Electrical Stimulation Achieves Stimulation of Small Fibres Selectively: A Simulation Study. *Physics in Medicine and Biology* 61, 4479–4490. doi: 10.1088/0031-9155/61/12/4479
- Otsuru, N., Inui, K., Yamashiro, K., Miyazaki, T., Ohsawa, I., Takeshima, Y., et al. (2009). Selective Stimulation of C Fibers by an Intra-Epidermal Needle Electrode in Humans. *The Open Pain Journal* 2, 53–56. doi: 10.21774/1876386300902010053
- Poulsen, A. H., Tigerholm, J., Meijs, S., Andersen, O. K., and Mørch, C. D. (2020). Comparison of Existing Electrode Designs for Preferential Activation of Cutaneous Nociceptors. *Journal of Neural Engineering* 17, 036026. doi: 10.1088/1741-2552/ab85b1
- Rag e, M., Van Acker, N., Facer, P., Shenoy, R., Knaepen, M. W. M., Timmers, M., et al. (2010). The Time Course of CO<sub>2</sub> Laser-Evoked Responses and of Skin Nerve Fibre Markers after Topical Capsaicin in Human Volunteers. *Clinical Neurophysiology* 121, 1256–1266. doi: 10.1016/j.clinph.2010.02.159
- Rattay, F. (1999). The Basic Mechanism for the Electrical Stimulation of the Nervous System. *Neuroscience* 89, 335–346.
- Reilly, D. M., Ferdinando, D., Johnston, C., Shaw, C., Buchanan, K. D., and Green, M. R. (1997). The Epidermal Nerve Fibre Network: Characterization of Nerve Fibres in Human Skin by Confocal Microscopy and Assessment of Racial Variations. *British Journal of Dermatology* 137, 163–170. doi: 10.1046/j.1365-2133.1997.18001893.x
- Reilly, J. P. (1989). Peripheral Nerve Stimulation by Induced Electric Currents: Exposure to Time-Varying Magnetic Fields. *Medical & Biological Engineering & Computing* 27, 101–110. doi: 10.1007/BF02446217
- Rohracher, H. (1935). *Ueber Subjektive Lichterscheinungen Bei Reizung Mit Wechselstr omen*. J. A. Barth. \*\*city.
- Roth, A., and van Rossum, M. C. W. (2013). “Modeling Synapses,” in *Computational Modeling Methods for Neuroscientists*, ed. E. De Schutter (Cambridge, MA: MIT Press), 139–160. doi: 10.7551/mitpress/9780262013277.003.0007
- Schmid, G., Cecil, S., and  uberbacher, R. (2013). The Role of Skin Conductivity in a Low Frequency Exposure Assessment for Peripheral Nerve Tissue According to the ICNIRP 2010 Guidelines. *Physics in Medicine and Biology* 58, 4703–4716. doi: 10.1088/0031-9155/58/13/4703
- Simons-Weidenmaier, N. S., Weber, M., Plappert, C. F., Pilz, P. K. D., and Schmid, S. (2006). Synaptic Depression and Short-Term Habituation Are Located in the Sensory Part of the Mammalian Startle Pathway. *BMC Neuroscience* 7:38. doi: 10.1186/1471-2202-7-38
- Sweeney, J. D., Mortimer, J. T., and Durand, D. (1987). “Modeling of Mammalian Myelinated Nerve for Functional Neuromuscular Electrostimulation,” in *IEEE 97th Annual Conf. Engineering in Medicine Biology Society*, Vol. 9, (Boston), 1577–1578.
- Tanaka, S., Gomez-Tames, J., Wasaka, T., Inui, K., Ueno, S., and Hirata, A. (2021). Electrical Characterisation of A $\delta$ -Fibres Based on Human In Vivo Electrostimulation Threshold. *Frontiers in Neuroscience* 14:588056. doi: 10.3389/FNINS.2020.588056
- Taniguchi, M., Cedzich, C., and Schramm, J. (1993). Modification of Cortical Stimulation for Motor Evoked Potentials under General Anesthesia: Technical Description. *Neurosurgery* 32, 219–226.
- Turi, Zs, Ambrus, G. G., Janacsek, K., Emmert, K., Hahn, L., Paulus, W., et al. (2013). Both the Cutaneous Sensation and Phosphene Perception Are Modulated in a Frequency-Specific Manner during Transcranial Alternating Current Stimulation. *Restorative Neurology and Neuroscience* 31, 275–285.
- Vallbo, A. B., Hagbarth, K. E., Torebj ork, H. E., and Wallin, B. G. (1979). Somatosensory, Proprioceptive, and Sympathetic Activity in Human Peripheral Nerves. *Physiological Reviews* 59, 919–957.
- Weiss, T., Straube, T., Boettcher, J., Hecht, H., Spohn, D., and Miltner, W. H. R. (2008). Brain Activation upon Selective Stimulation of Cutaneous C- and Adelta-Fibers. *NeuroImage* 41, 1372–1381. doi: 10.1016/j.neuroimage.2008.03.047

**Conflict of Interest:** The authors declare that the research was conducted in the absence of any commercial or financial relationships that could be construed as a potential conflict of interest.

Copyright   2021 Tanaka, Gomez-Tames, Inui, Ueno, Hirata and Wasaka. This is an open-access article distributed under the terms of the Creative Commons Attribution License (CC BY). The use, distribution or reproduction in other forums is permitted, provided the original author(s) and the copyright owner(s) are credited and that the original publication in this journal is cited, in accordance with accepted academic practice. No use, distribution or reproduction is permitted which does not comply with these terms.